Applied Physics Letters ARTICLE scitation.org/journal/apl

Noninvasive photoluminescence imaging of silicon PV modules in daylight

Cite as: Appl. Phys. Lett. **120**, 244102 (2022); doi: 10.1063/5.0097576
Submitted: 29 April 2022 · Accepted: 24 May 2022 ·
Published Online: 15 June 2022

M. Vuković,[a] M. Jakovljević, A. S. Flø, E. Olsen, and I. Burud

AFFILIATIONS

Faculty of Science and Technology, Norwegian University of Life Sciences, Ås, Norway

[a]Author to whom correspondence should be addressed: marija.vukovic@nmbu.no

ABSTRACT

Outdoor photoluminescence imaging on field-deployed solar cell modules has been conducted to an increasing extent in recent years. Photoluminescence images provide more details about defects than thermal infrared images, while the imaging procedure has the potential to be faster than electroluminescence imaging because it does not require electrical connection to the modules. However, when conducted with sunlight excitation, it is based on lock-in technique, which implies switching between the modules' two operating points. This often results in the need to connect additional electrical equipment dimensioned for the task and leads to production disruption for the investigated modules. The present study demonstrates image acquisition based on the string inverter's ability to sweep the IV curve. The advantage of this approach is twofold. This is a noninvasive method, which only requires imaging apparatus and, therefore, allows for a flexible imaging procedure on the string, module, or cell level without having to take into account additional equipment. Furthermore, photoluminescence images spanning the whole IV curve can be obtained during one sweep, as opposed to obtaining images in two operating points when using lock-in technique. Such image series can be used to investigate the state of the cells and modules by looking at the photoluminescence images acquired on different current extraction levels. This has been done for a healthy string and a broken module.

Images of photoluminescence (PL) emitted from silicon photovoltaic (PV) cells and modules can be acquired due to the radiative band-to-band recombination of charge carriers over the bandgap at 1150 nm.[1] This signal can reveal different parameters affecting solar cell performance and is a valuable tool for the PV industry.[1] PL images of modules collected outdoor have been studied to an increasing extent in recent years,[2–8] and they can reveal a variety of faults that might affect their performance, such as cracks,[3,4,6] potential induced degradation,[5] "snail trails,"[5] ethylene vinyl acetate (EVA) degradation,[5] bypass diode failures,[4,5] and regions affected by series resistance losses.[2–5,8] The advantage of outdoor PL imaging is that the procedure can potentially be notably faster than electroluminescence (EL) imaging because electrical connection to a PV system is no prerequisite as it is for EL imaging. Additionally, PL images, similar to EL images, provide more information than thermal infrared images.[9]

When PL imaging is conducted with sunlight excitation, the weak radiative band-to-band signal is not obtainable due to the reflected sunlight recorded by the camera, unless the image acquisition is carried through together with the modulation of the PV system's operating point.[2–4,6–8] Approaches developed so far are mostly dependent on the equipment dimensioned for imaging a certain number of modules.[2,4,7,10] In that way, PL imaging ceases to be a contactless imaging method, it causes interference with the production process, and it makes it harder to make spontaneous decisions in the field.

We demonstrate a noninvasive method for PL imaging of PV modules, which takes advantage of an integrated functionality of string inverters, namely, the IV curve sweep. Connection with the PV system is not necessary. The only equipment is the imaging apparatus allowing for flexibility to image on the string, module, or cell level. The validity of a PL image obtained in this way is discussed compared to an EL image. Advantages of a data set spanning the whole IV curve are demonstrated.

The PL signal intensity is dependent on the level of current extraction during the IV curve sweep. The extracted current density J of an area A of a solar cell, which behaves as an ideal diode, is given by

$$J = J_{SC} - J_0 \exp^{\frac{V_{d,A}}{V_t}}, \quad (1)$$

where J_{SC} is the short circuit (SC) current density and J_0 is the total dark current density.[11,12] The PL signal of the area A is given by

$$PL_A = C \exp^{\frac{V_{d,A}}{V_t}} + PL_{offset,A}, \quad (2)$$

where C is a calibration constant accounting for the carrier lifetime of the cell, the optical characteristics, and geometry; $V_{d,A}$ is the diode voltage of the same area; V_t is the thermal voltage; and $PL_{offset,A}$ is the PL signal caused by diffusion-limited carriers.[12,13] Solving Eq. (2) for $V_{d,A}$ and substituting in Eq. (1) result in

$$J = J_{SC} - \frac{J_0}{C}(PL_A - PL_{offset,A}). \quad (3)$$

The levels of current extraction and the PL signal intensities in two different operating points are given by

$$J_1 = J_{SC1} - \frac{J_{01}}{C_1}(PL_{A1} - PL_{offset1,A}) \quad (4)$$

and

$$J_2 = J_{SC2} - \frac{J_{02}}{C_2}(PL_{A2} - PL_{offset2,A}). \quad (5)$$

Since the calibration constant C can be determined from an image in the open circuit condition and the open circuit voltage,[11,12] $C_1 = C_2 = C$. The illumination conditions are considered unchanged during the acquisition of two images, and therefore, $J_{SC1} = J_{SC2} = J_{SC}$. The dark current density is assumed $J_{01} = J_{02} = J_0$. Since $PL_{offset,A}$ is obtained with an image in the SC condition,[11,12] $PL_{offset1,A} = PL_{offset2,A} = PL_{offset,A}$. Subtracting Eq. (5) from Eq. (4) and solving for the difference in PL signal intensity result in

$$PL_{A2} - PL_{A1} = \frac{C}{J_0}(J_1 - J_2). \quad (6)$$

This relationship shows that the difference in the PL signal intensity between two operating conditions, $\Delta PL = PL_2 - PL_1$, is linearly proportional to the difference in the extracted current density. The intensity of the PL signal in condition 2, PL_2, is higher than in condition 1, PL_1, at the same time as the current density J_2 is lower than J_1. In the following, the average PL signal intensity of an area is analyzed as a function of its extracted current.

Images were acquired in this study during measurement of a part of the IV curve performed by the string inverter Fronius Primo 3.0[14] connected to three bifacial passivated emitter and rear cell (PERC) modules (JA Solar JAM72D20) in series as shown in Fig. 1. This built-in functionality is a part of the string inverter's intelligent shade management with the aim of searching for the global maximum power point (MPP) and is realized by sweeping the IV curve every 10 min. The camera was positioned in front of the modules connected to the inverter, and 200 000 images were collected during approximately 20 min. In that period, two IV curve sweeps took place.

The imaging was conducted with a short-wave infrared camera of type Raptor Photonics Owl 640S with an InGaAs detector, an optical range of 900–1700 nm, and 640 × 512 resolution. An optical bandpass filter by Edmund Optics with the wavelength range of 1100–1150 nm and the optical density of ≥ 4.0 is used in order to filter out the reflection detected outside the range of the emitted PL signal. The integration time of 0.3 ms and the frame rate of 167 Hz (the acquisition time of 6 ms) allowed for approximately 330 images to be collected during one sweep.

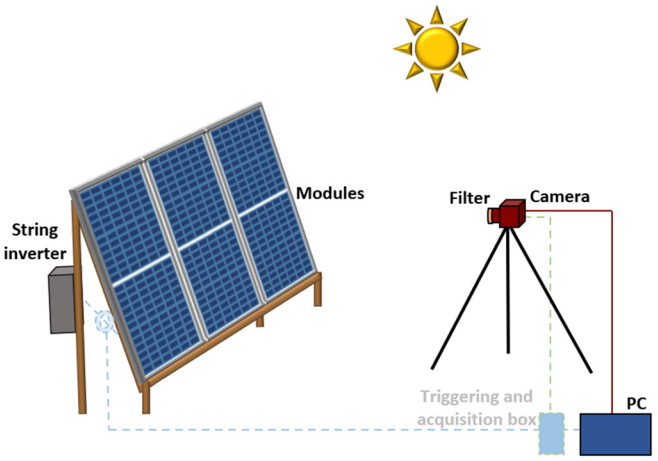

FIG. 1. Experimental setup for PL imaging and current measurements for the PV string consisting of three bifacial modules.

In order to illustrate the IV curve sweep in this study, current had to be recorded. This was done at the same time as the images were collected using a triggering and acquisition box, as illustrated in Fig. 1. The box triggered the camera and recorded the current. This part of the equipment, illustrated with light color and dashed lines, is otherwise not necessary because the increase in the PL signal intensity, i.e., the pixel values, is a sign of the IV curve sweep taking place.

One IV curve sweep during which the images were acquired is displayed in Fig. 2. Figure 2(a) shows the string current at the MPP at approximately 11 A when the sudden drop below 5 A is measured at 12 h 23 min. The current drop is enlarged in Fig. 2(b) with the values on the x-axis sampled in milliseconds. It shows that it takes approximately 2 s for the inverter to sweep the IV curve. The current data are overlaid with the average pixel count per image as a function of time, which is the sum of reflection from the modules and the PL signal. The increase in the total signal detected is due to the increase in the PL signal at the time of the current fall.

The blue and red areas in Fig. 2(b) mark the images selected for the calculation of one difference PL image, ΔPL. They are chosen so that they might give a ΔPL image with the highest difference in PL signal. The two areas are selected based on where the PL signal is at its strongest (top of the blue curve) and at its weakest (dip in the blue curve). The calculation was performed by averaging and subtracting 80 images in the red region from 80 images in the blue region. The obtained ΔPL image is compared with the EL images of the modules acquired in the dark with SC current, EL_{SC}.

In order to further investigate the quality and possibilities of these data set, the result in Eq. (6) is tested for the images marked in blue and red in Fig. 2(c). These areas are defined in order to produce not one, but a sequence of ΔPL images. Averaging over the images in the blue region results in a PL_2 image [Eq. (6)] with the lowest current for five images. Looping through the red area by choosing five new images with every step results in 14 PL_1 images. The interval size of five images was chosen as a trade-off between improving the quality of ΔPL images through averaging and obtaining a data set with more points. The red region starts at the SC condition and is defined so that it does not comprise redundant data, i.e., images taken in the same

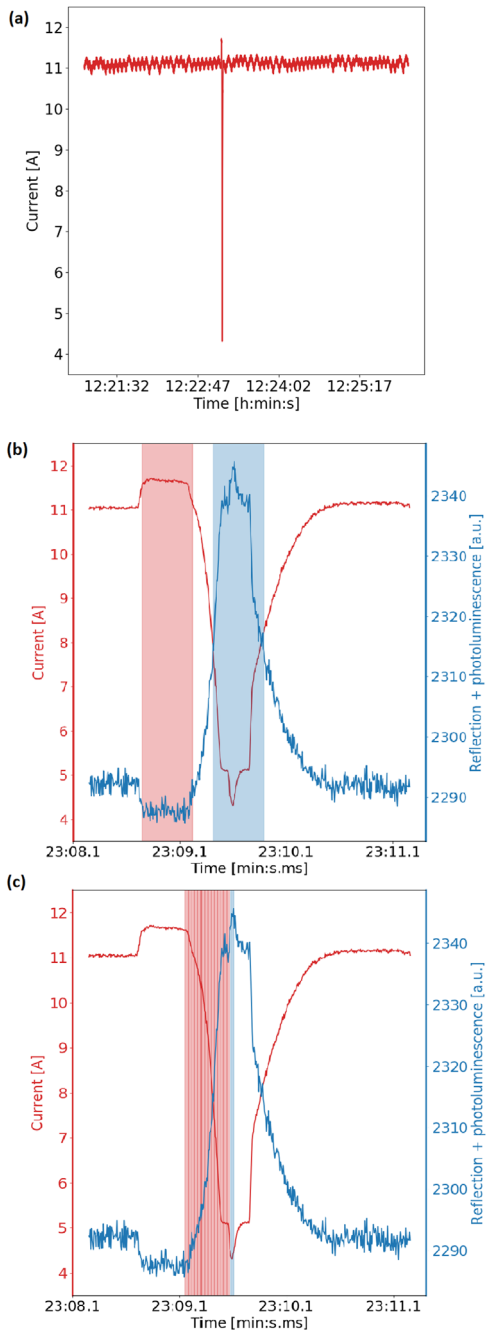

FIG. 2. Current displayed as a function of time showing a brief fall at 12 h 23 min (a). Time sequence between 12 h 23 min 8 s and 12 h 23 min 11 s shows the shape of the current fall and the increasing signal from the modules. The blue and red areas mark the selected images resulting in a ΔPL image (b). The same enlarged time sequence with red and blue regions mark the images chosen to test the result in Eq. (6) (c).

operating condition. For every ΔPL image obtained, the difference in extracted current is calculated.

The ΔPL image of the string obtained as described in Fig. 2(b) is shown in Fig. 3(a). Three separate EL_{SC} images are shown in Fig. 3(b).

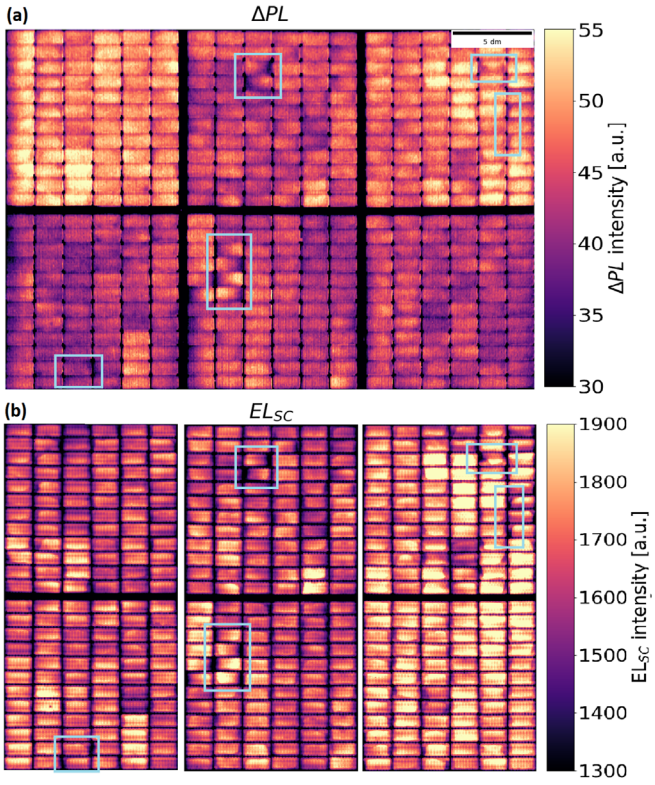

FIG. 3. ΔPL image of a string consisting of three bifacial modules connected in series (a) and three EL_{SC} images of the modules (b).

The pixel values differ on the two scales since they represent the intensity of different signals. The EL images show three modules, which appear to be in a good state. The ΔPL image is in accordance with this observation. A few areas, which display lower intensity values in the EL images, are marked with blue squares in Fig. 3(a) and Fig. 3(b). They appear to be areas with dark color, i.e., increased series resistance, which are visible to a smaller or greater extent in the ΔPL image.

The color distribution on the ΔPL image in Fig. 3(a) and EL_{SC} images in Fig. 3(b) differs in such a way that the ΔPL values in the upper halves of the two modules on the sides seem to be higher than in the lower halves of the same modules. The upper halves are elevated from the ground, and for the bifacial modules, this leads to increased gain,[15] which might be the case here. Why this is not so clearly visible for the upper part of the middle module could be because it is in the middle and less diffuse light reached it at the back in the moment of imaging.

The data points obtained based on Eq. (6) and Fig. 2(c), $PL_2 - PL_1$ as a function of difference in current, are plotted in Fig. 4. They are fitted with a linear model with the coefficient of determination $R^2 = 0.9987$ having the intercept point of -0.016. The intercept point very close to zero is in accordance with Eq. (6). The modules satisfy the assumption about an ideal diode model since they display a linear relationship between the ΔPL and difference in current extraction. This confirms the observations in Fig. 3 that the modules are in a good state and not affected by any serious resistance problems. The result in Fig. 4 also shows that the data set collected can be used to produce not

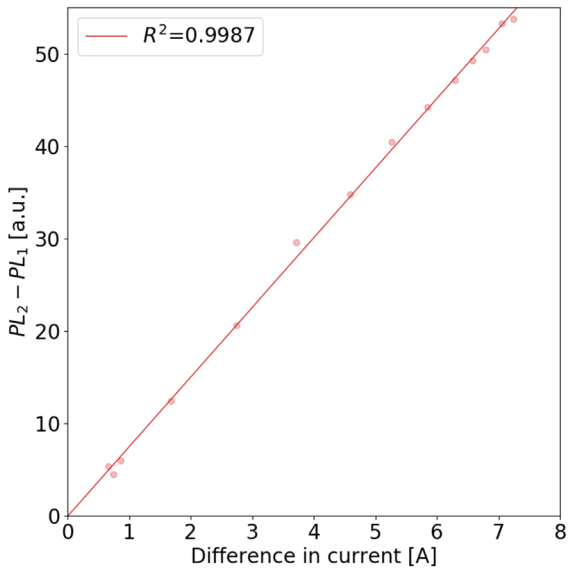

FIG. 4. Linear regression model y = 7.54x − 0.067 fitted to the average pixel count as a function of current difference for 14 images.

only one Δ*PL* image but also several of them with different signal intensities. This makes it possible to assess modules with defects into greater detail.[3,4]

In order to investigate how useful Δ*PL* images obtained with different levels of current extraction might be, the imaging procedure has been conducted on a broken bifacial module. This is illustrated in Fig. 5. An EL_{SC} image is shown in Fig. 5(a), while two Δ*PL* images are shown in Figs. 5(b) and 5(c). The raw images in Figs. 5(b) and 5(c) were acquired with an average current of 3.49 A/5.74 A and 5.74 A/7.99 A, respectively, meaning that the difference in current extraction is 2.25 A for both images. The Δ*PL* image in Fig. 5(b) is quite similar to the EL image with respect to color distribution, while the image in Fig. 5(c) differs. This is particularly the case for the two lower left columns. The intact cells of this sub-string have high values in Figs. 5(a) and 5(b). However, the same two columns behave differently in Fig. 5(c) and have considerably lower values compared to the rest of the module.

Given the irradiation level at the time of imaging, the MPP current for this module was at 7.32 A. This means that the Δ*PL* image in Fig. 5(b) was obtained with images taken when the current was in the lower part of the IV curve, while the image in Fig. 5(c) was obtained with one current level above and one below the MPP. Very low Δ*PL* values in Fig. 5(c) for the lower left sub-string might mean that the current levels above the MPP cannot be extracted equally well as currents below the MPP. Further analysis of the state of this module is needed. This particular case shows how different Δ*PL* images might give diverging information. The advantage of conducting image acquisition with the IV curve sweep is that a whole range of Δ*PL* images is obtained without having to invest any additional effort in acquiring them.

Photoluminescence images of PV modules collected outdoor with sunlight excitation can provide useful information about the field-deployed modules. Removing the need for additional equipment and disturbance in power production contributes to a more efficient imaging. The present study demonstrates a method, which takes advantage of already existing PV system equipment in the field. A series of images can be collected during the string inverter's IV curve measurement and result in a whole range of PL images. They can be a useful tool to analyze the nature of the defects that the modules might be affected by. This method allows for diagnostic imaging with a high throughput on the string level before a more targeted imaging is conducted on a module or cell level.

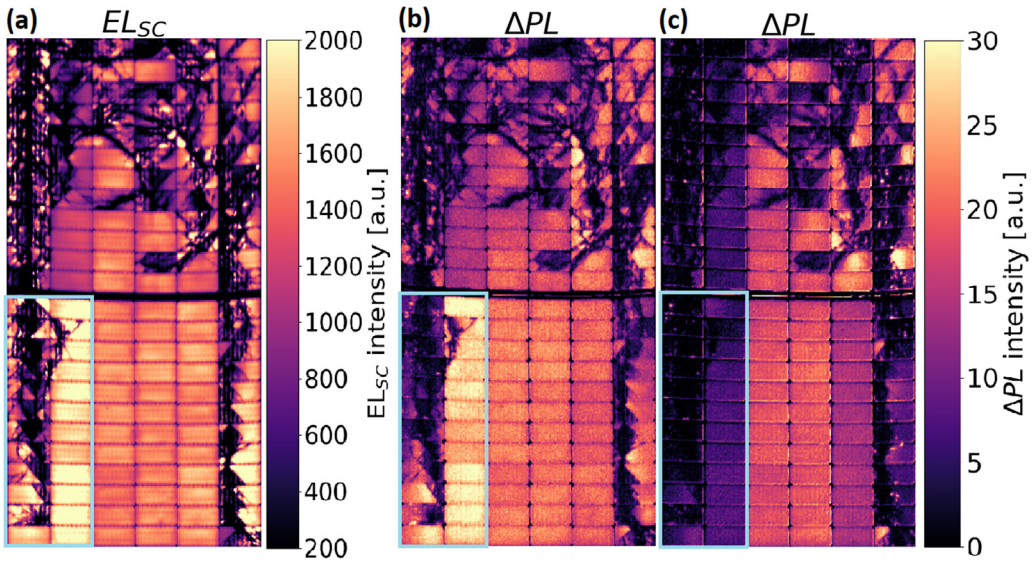

FIG. 5. EL_{SC} image of a broken bifacial module (a), Δ*PL* image obtained with PL_1 and PL_2 taken with a difference in current extraction of 5.74 A − 3.49 A = 2.25 A (b), and Δ*PL* obtained with the same difference in current extraction 7.99 A − 5.74 A = 2.25 A (c).

This work was performed within The Norwegian Research Center for Sustainable Solar Cell Technology (FME SUSOLTECH, Project No. 257639/E20). The center is co-sponsored by the Research Council of Norway and its research and industry partners.

AUTHOR DECLARATIONS

Conflict of Interest

The authors have no conflicts to disclose.

DATA AVAILABILITY

The data that support the findings of this study are available from the corresponding author upon reasonable request.

REFERENCES

[1]E. Olsen and A. Flø, "Spectral and spatially resolved imaging of photoluminescence in multicrystalline silicon wafers," Appl. Phys. Lett. **99**, 011903 (2011).
[2]L. Stoicescu, M. Reuter, and J. Werner, "DaySy: Luminescence imaging of PV modules in daylight," in *29th European Photovoltaic Solar Energy Conference and Exhibition* (EU PVSEC, 2014), pp. 2553–2554.
[3]T. Silverman, M. Deceglie, K. VanSant, S. Johnston, and I. Repins, "Illuminated outdoor luminescence imaging of photovoltaic modules," in *IEEE 44th Photovoltaic Specialist Conference* (IEEE, 2017), pp. 3452–3455.
[4]R. Bhoopathy, O. Kunz, M. Juhl, T. Trupke, and Z. Hameiri, "Outdoor photoluminescence imaging of solar panels by contactless switching: Technical considerations and applications," Prog. Photovolt Res. Appl. **28**, 217–212 (2020).
[5]B. Doll, J. Hepp, M. Hoffmann, R. Schüler, C. Buerhop-Lutz, I. Peters, J. Hauch, A. Maier, and C. Brabec, "Photoluminescence for defect detection on full-sized photovoltaic modules," IEEE J. Photovoltaics **11**, 1419–1411 (2021).
[6]L. Köster, A. Astigarraga, S. Lindig, A. Louwen, M. Antinori, D. Moser, and G. Manzolini, "Quality assurance of the photovoltaic power plants installation stage—A complementary strategy based of photoluminescence and steady-state thermography," in *38th European Photovoltaic Solar Energy Conference and Exhibition* (EU PVSEC, 2021), pp. 1042–1050.
[7]O. Kunz, G. Rey, M. Juhl, and T. Trupke, "High throughput outdoor photoluminescence imaging via PV string modulation," in *48th IEEE Photovoltaic Specialists Conference* (2021), pp. 346–350.
[8]M. Vuković, I. Høiaas, M. Jakovljević, A. Flø, E. Olsen, and I. Burud, "Photoluminescence imaging of silicon modules in a string," Prog. Photovolt Res. Appl. **30**, 436–446 (2022).
[9]W. Herrmann, G. Eder, B. Farnung, G. Friesen, M. Köntges, B. Kubicek, O. Kunz, H. Liu, D. Parlevliet, I. Tsanakas, and J. Vedde, "Qualification of photovoltaic (PV) power plants using mobile test equipment," Photovoltaic Power System Programme 13, Report No. IEA-PVPS T13-24:2021 (International Energy Agency, 2021).
[10]M. Guada, Moretón, S. Rodríguez-Conda, L. Sánchez, M. Martínez, M. González, J. Jiménez, L. Pérez, V. Parra, and O. Martínez, "Daylight luminescence system for silicon solar panels based on a bias switching method," Energy Sci. Eng. **8**, 3839–3853 (2020).
[11]T. Trupke, M. Abbott, and E. Pink, "Spatially resolved series resistance of silicon solar cells obtained from luminescence imaging," Appl. Phys. Lett. **90**, 093506 (2007).
[12]Y. Augarten, T. Trupke, M. Lenio, J. Bauer, O. Breitenstein, J. Weber, and R. Bardos, "Luminescence shunt imaging: Qualitative and quantitative shunt images using photoluminescence imaging," in *24th European Photovoltaic Solar Energy Conference* (EU PVSEC, 2009), pp. 27–31.
[13]C. Shen, "Power loss analysis via photoluminescence," Ph.D. dissertation (UNSW, 2014).
[14]F. S. Energy, "Dynamic peak manager: Profitable PV systems despite shading, 2022" (last accessed April 17, 2022).
[15]X. Sun, M. Khan, C. Deline, and M. Alam, "Optimization and performance of bifacial solar modules: A global perspective," Appl. Energy **212**, 1601–1610 (2018).